Methods for Compensation of the Light Attenuation With Depth of Images Captured by a Confocal Microscope

MARTIN ČAPEK,[1,2]* JIŘÍ JANÁČEK,[1] AND LUCIE KUBÍNOVÁ[1]
[1]*Institute of Physiology, Academy of Sciences of the Czech Republic, 142 20 Prague, 4-Krč, Czech Republic*
[2]*Faculty of Biomedical Engineering, Czech Technical University in Prague, 272 01 Kladno 2, Czech Republic*

KEY WORDS confocal microscopy; light attenuation; hardware adjustment; image enhancement; histogram warping

ABSTRACT A confocal laser scanning microscope (CLSM) enables us to capture images from a biological specimen in different depths and obtain a series of precisely registered fluorescent images. However, images captured from deep layers of the specimen may be darker than images from the topmost layers because of light loss distortions. This effect causes difficulties in subsequent analysis of biological objects. We propose a solution using two approaches: either an online method working already during image acquisition or an offline method assisting as a postprocessing step. In the online method, the gain value of a photomultiplier tube of a CLSM is controlled according to the difference of mean image intensities between the reference and currently acquired image. The offline method consists of two stages. In the first stage, a standard histogram maintaining relative frequencies of gray levels and improving brightness and contrast is created from all images in the series. In the second stage, individual image histograms are warped according to this standard histogram. The methods were tested on real confocal image data captured from human placenta and rat skeletal muscle specimens. It was shown that both approaches diminish the light attenuation in images captured from deep layers of the specimen. *Microsc. Res. Tech. 69:624–635, 2006.*

INTRODUCTION

A confocal laser scanning microscope (CLSM) is a noninvasive tool that gives possibility to obtain a stack (series) of fluorescent optical sections, i.e., a three-dimensional (3D) volume, representing an investigated biological specimen through optical sectioning and scanning of 2D confocal planes (Pawley, 1995). Unfortunately, fluorescent image intensities from a CLSM suffer from light loss distortions that can be described by two main effects—light aberration and photobleaching.

The effect of photobleaching, causing an irreversible destruction of fluorescence within a stained specimen, can be only partially reduced by adding antioxidants to the biological specimen or by decreasing the laser light intensity and/or the time of image exposure. It is also difficult to stain a thick specimen by fluorophores evenly. Thus, the staining intensity may vary in different depths within the specimen causing the light intensity attenuation.

Light aberrations include chromatic and spherical aberrations introduced by the optical elements in the microscope, refractive-index mismatch between the objective and the specimen, and aberrations resulting from focusing and light propagation through a turbid specimen—light scattering, refraction, and absorption.

Chromatic and spherical aberrations of the optical elements of a CLSM cause distortion of focus, which leads to a decrease in excitation intensity. A mismatch in the refractive index among the objective, used immersion fluid and the specimen results in an incorrect scaling of the image stack in the axial direction and in increasing spherical aberrations, which broadens the point spread function (PSF) of a CLSM. The PSF width increases with focusing deeper inside the specimen and causes spreading of the excitation energy over a larger volume, thus reducing the fluorescence signal. Objects in a specimen comparable to or smaller than the wavelength scatter both excitation and emission light. Objects larger than the wavelength and having a different refractive index from their environment partially refract both excitation and emission photons. Scattering and refraction depend on the objects morphology and density; therefore, these effects vary for different specimens. Moreover, small absorption of excitation photons in a specimen can be observed, especially in a single-photon microscopy.

All described effects influence the PSF size, reduce the light intensity in the focal region, and thus reduce the resulting fluorescence signal (Diaspro, 2002). The problem of the distorted PSF can be partially solved by image deconvolution techniques (de Monvel et al., 2001; Difato et al., 2004; Verveer et al., 1999) which represent an effective approach to decrease blur in 3D

*Correspondence to: Martin Čapek; Institute of Physiology, Academy of Sciences of the Czech Republic, Vídeňská 1083, 142 20 Prague 4 – Krč, Czech Republic. E-mail: capek@biomed.cas.cz

Received 31 August 2005; accepted in revised form 2 January 2006

Contract grant sponsor: Czech Technical University in Prague, Ministry of Education, Youth and Sports of the Czech Republic; Contract grant numbers: MSM6840770012 and LC06063; Contract grant sponsor: Academy of Sciences of the Czech Republic; Contract grant numbers: A100110502, A600110507, A500200510, KJB6011309, AV0Z 50110509; Contract grant sponsor: Grant Agency of the Czech Republic; Contract grant numbers: 304/05/0153.

DOI 10.1002/jemt.20330

Published online 1 June 2006 in Wiley InterScience (www.interscience.wiley.com).

microscopic images and improve signal-to-background contrast. However, they do not improve the effect of the light attenuation with depth. As a consequence, images captured from deep layers of the specimen may be darker than images from the topmost layers. This causes problems in subsequent image analysis, segmentation, and 3D visualization of objects.

A lot of articles devoted to intensity variations correction have been published. In computer vision, this problem refers to correcting optical flow among images of the scene obtained at two or more different times (Negahdaripour, 1998; Negahdaripour and Yu, 1993). The authors apply a general model in which the x, y flow field and additive and multiplicative intensity relationships must be estimated at every pixel. However, this approach is time-consuming in the case of high resolution 3D microscopic images. A simplification of this general model has been described by Cox et al. (1995) who developed a method based on histogram warping (HSWP) that is restricted to the case where a global, spatially invariant, nonlinear, monotonically increasing relationship between the intensities of two images exists. This technique is closely related to works in histogram specification (Gonzales and Woods, 1993; Zhang, 1992).

Another approach lies in the least squares optimization with brightness and contrast being optimized parameters exploiting all image pixel values (Kervrann et al., 2004; Periaswamy and Farid, 2003). These techniques are generally highly sensitive to noise present in images, which is practically always the case of CLSM images. The method by Kervrann et al. (2004) tried to overcome this difficulty by applying an iteratively reweighted least squares method. In medical imaging, methods for standardization of the gray scale of MRI (magnetic resonance imaging) images have been published (Nyúl and Udupa, 1998; Nyúl et al., 2000). They are based on remapping image intensities by matching landmarks found in image histograms.

Some articles deal with the light attenuation compensation in fluorescence microscopy. Many of them use especially the exponential decay law for modeling the light attenuation with depth because of scattering, absorption, and photobleaching (Ghauharali and Brakenhoff, 1998; Ghauharali and Brakenhoff, 2000; Kervrann et al., 2004; Markham and Conchello, 2001; Rodenacker et al., 2001; Sun et al., 2004). A method based on the study of a stack of 2D histograms formed from each consecutive pair of optical sections was applied to calculate the attenuation factor (Liljeborg et al., 1995). Another method that integrates the attenuation along all light paths within the numerical aperture of the objective was proposed by Margadant et al. (1996). Compensation of brightness supposing linear decay of mean image intensities using a least squares solution was employed by Wahlby et al. (2004).

In the present study, we propose two methods for compensation of the light attenuation with depth. The first one is an online method applied during image acquisition of optical sections of a specimen. It adjusts the gain value of a photomultiplier tube of a CLSM, according to the difference of mean image intensities between the reference and currently scanned image in a given channel.

The second method represents an offline method used as a postprocessing step. During its development, we were inspired especially by methods described by Cox et al. (1995) and Nyúl et al. (2000). We developed a general approach consisting of two stages. In the first stage, a standard histogram, maintaining relative frequencies of gray levels and reducing the light attenuation, is created from all optical sections in a stack. In the next stage, image histograms of optical sections are warped according to the standard histogram to achieve as uniform as possible contrast and brightness of images in the stack.

The aim of the described methods is to obtain better visualization of data and a possibility to simplify segmentation methods applied to acquired images. For example, a single threshold for segmentation of objects in the whole stack could be then applied if specific staining of structures of interest is used. To our knowledge, no such algorithms are available in today's commercial software packages.

MATERIALS AND METHODS

All following experiments were performed using a Leica SP2 AOBS confocal laser scanning microscope (CLSM) controlled by a personal computer equipped with the proprietary Leica Confocal Software. Stacks of optical sections were captured using an HCX PL APO CS 40.0 × 1.25 oil objective.

Figures 1 and 2 show every sixth image of the series of optical sections of human placenta and rat skeletal muscle fibers, respectively. Excitation wavelength applied was 488 nm for both stacks. Emission wavelengths ranged from 500 to 535 nm for the placenta specimen and from 533 to 598 nm for the muscle specimen. The placenta specimen was prepared according to Jirkovská et al. (2002) and the rat muscle specimen according to Čebašek et al. (2004). To demonstrate high applicability of our methods, the first stack represents a specimen with an object covering majority of the area of images, while the second one represents a biological specimen characterized by a high portion of background. The upper left image of both figures comes from the topmost layer of the specimens whereas the bottom right image from the deepest layer. The heights of the stacks were about 21 μm and 42 μm, respectively.

The optical sections differ not only by their intensity levels and contrast, but their appearance is changing during focusing through the structure. This fact complicates the intensity compensation problem. It is impossible to apply correction methods based on evaluation of correspondence and intensity of individual objects, e.g., registration-based procedures.

The proposed online and offline methods are described below.

Online Method

The online method was implemented using Macro Developer included in Leica Confocal Software package. Macro Developer provides possibility to develop macros in Visual Basic programming language to adjust CLSM hardware.

The main, important parameter that can be adjusted during an optical section acquisition is the gain of a photomultiplier tube. This gain, expressed by voltage in Volts, reflects amplification of a detected signal com-

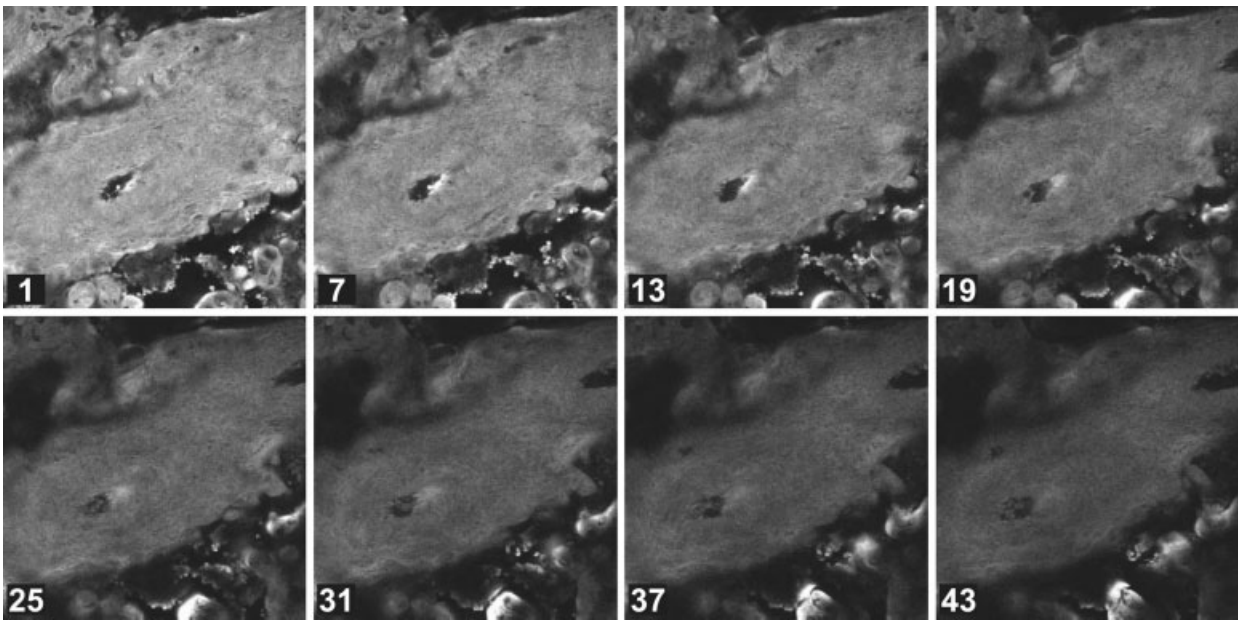

Fig. 1. Subset of a series of optical sections of a human placenta captured by a confocal microscope. The distance between sections in the subset is about 3 μm. The numbers in the figure depict numerical order of optical sections in the full series.

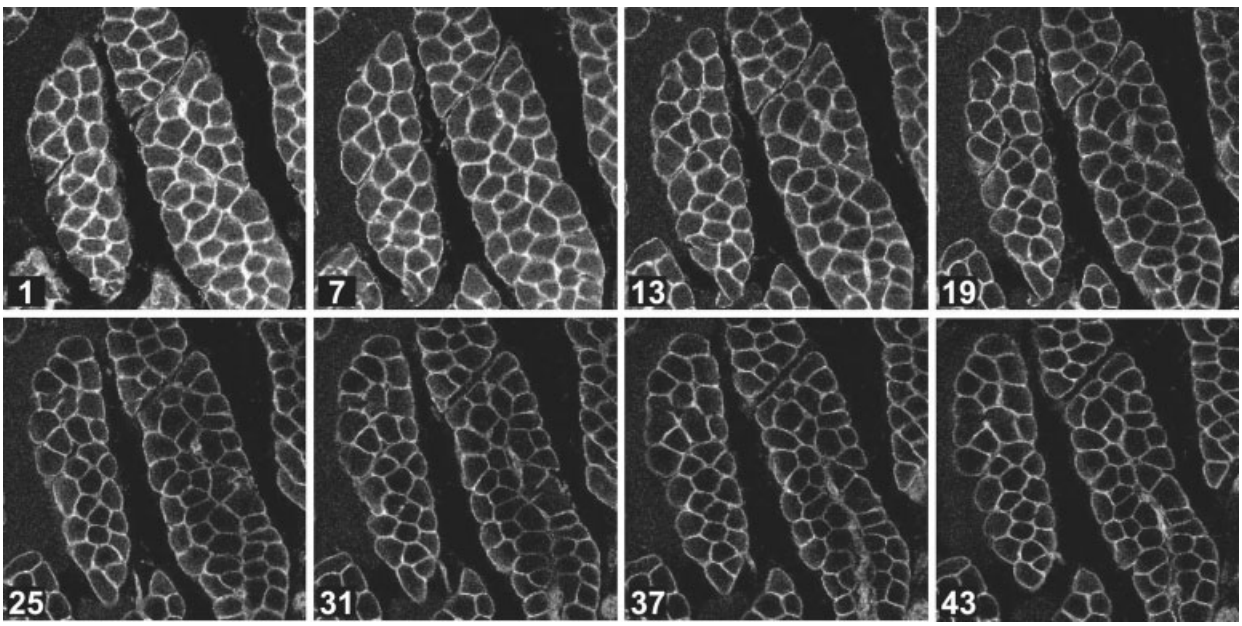

Fig. 2. Subset of a series of confocal optical sections of rat skeletal muscle fibers captured by a confocal microscope. The distance between sections in the subset is about 6 μm. The numbers depict numerical order of optical sections in the full series.

ing from the given channel during scanning, i.e., the higher the gain sets, the more amplified detected signal is obtained.

We developed a macro called SCOM (Series Capture Optimization Macro) (see Figure 3). First, a user selects a reference image. This means that prior starting the macro, the user should capture at least one optical section of an investigated specimen. However, a better approach is to capture a whole stack of optical sections and then to select the best image from the stack as a reference one.

Next, the user selects a number of "testing shots," i.e., the number of evenly spaced confocal planes to be evaluated for the mean intensity level (MIL) of corresponding optical sections. During the computation process, the macro does not capture and optimize all optical sections of the specimen, but only this selected subset (see Figure 4). This approach decreases the

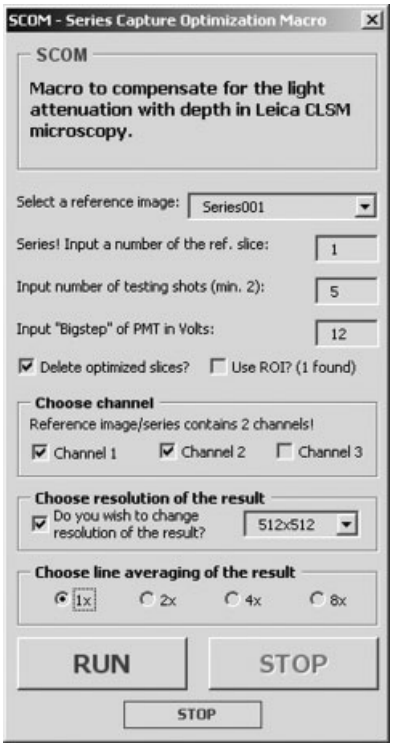

Fig. 3. Graphical user interface of the macro SCOM.

bleaching of used fluorochromes in the specimen and speeds up the macro by avoiding the repeated acquisition of all optical sections of the stack.

Then the macro performs optimization by seeking gain values yielding images of optical sections of the "testing shots" having the same intensity level. As a measure of the intensity level, we chose the MIL of an image. The main advantage of this measure lies in independency of its value on pixel positions, since images from different confocal planes differ.

To get the same value of MIL from the "testing shots," a value of the gain is optimized by "n-step search." This optimization strategy is based on decreasing searching steps to achieve a global minimum of the difference of MIL (DMIL) between the reference section and currently investigated section. In the case of our data shown in Figures 1 and 2, the value of n was 3. In the first level, n-step search seeks a minimum of DMIL using a high step of the gain (e.g., 12 Volts as shown in Fig. 3). After finding a minimal DMIL, the step is decreased and the optimization continues only in the vicinity of the previous result to achieve the minimum more precisely. Gain values of the "testing shots" being found, gain values of other confocal planes are computed by piecewise linear interpolation. Finally, the resulting stack of optical sections is captured with the obtained gain values.

If small or irregular objects are present in the specimen, it is possible to apply the macro only in a selected region of interest. To speed up the optimization, it is also possible to capture images of "testing shots" using a low resolution only, e.g., 128 $\times$ 128 pixels, and then for capturing the resulting series to select a high resolution, e.g., 512 $\times$ 512 pixels. If a high portion of noise

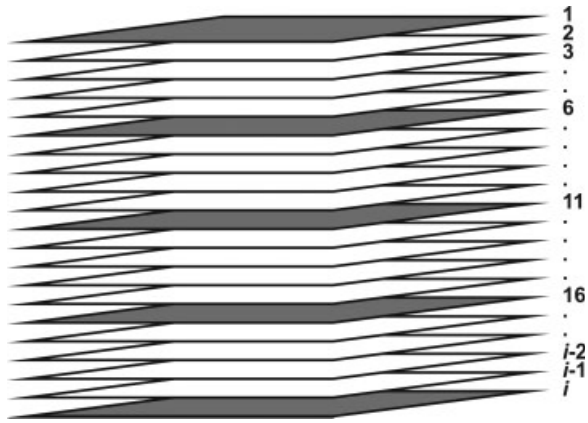

Fig. 4. Evenly spaced "testing shots" (dark gray) of a stack of i confocal planes.

is observed in optical sections prior to optimization, the averaging of image rows of the result can be employed (see Figure 3). The macro can be applied up to three channels that are optimized consecutively.

Offline Method

In the offline method, first, a standard histogram from a stack of images with different intensity levels and contrast is constructed. The aim is to obtain a histogram preserving a high contrast of optimally captured optical sections from top layers on one side and enabling contrast and brightness improvement of dark sections from deep layers on the other side. Then histograms of individual optical sections are warped according to the constructed standard histogram. Thus, all images in the stack are forced to have similar contrast and brightness.

Standard Histogram Construction. For construction of the standard histogram, we adapted the approach described by Nyúl et al. (2000) that is applied to gray-scale standardization of MRI images. This approach is based on matching landmarks in histograms. We chose the landmarks to be intensities corresponding to the minimum intensity, maximum intensity (noted m_1, m_2 in Fig. 6), and the nth percentiles of the image histogram, $n \in \{10, 20, \ldots, 90\}$, (noted $p_{10}, \ldots, p_{90}$). At the beginning, the algorithm calculates histograms of all optical sections in the stack and then evaluates landmarks in these histograms.

Further, unlike the original approach by Nyúl et al. (2000) matching the landmarks directly, our algorithm searches for the longest distance between two adjacent landmarks in one histogram, i.e., between the minimum intensity and the tenth percentile or between the tenth percentile and the twentieth percentile, etc. Maximal distances between landmarks are considered to preserve maximum image contrast. These distances are searched in all histograms. The maximal distances found (noted $M_1, M_2, \ldots, M_{10}$) are counted up and stretched to cover a grayscale of 256 levels (see Figure 5). This scale represents a standard scale according to which a standard histogram is to be computed. The breaks between rescaled maximal distances (noted L_0,

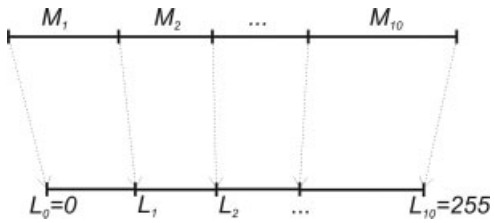

Fig. 5. Mapping maximal distances $M_1, M_2, \ldots, M_{10}$ found by the algorithm to a standard gray scale of 256 levels.

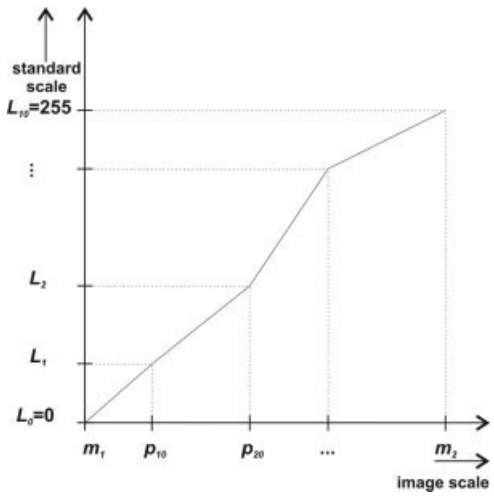

Fig. 6. Matching image landmarks with standard scale landmarks and piece-wise linear interpolation of new intensity values.

$L_1, L_2, \ldots, L_{10}$) are new landmarks of the standard scale.

New intensities of all image pixels of the stack are computed by matching landmarks of the standard scale and landmarks of individual image histograms. Image intensities between landmarks ($L_0, L_1, L_2, \ldots, L_{10}$) are piece-wise linearly interpolated, see Figure 6. The new intensity values are accumulated in the standard histogram. Since frequencies in bins of the standard histogram correspond to the whole stack, they are then adjusted to the size of one optical section.

Histogram Warping. Histogram warping (HSWP) (Cox et al., 1995) is a method trying to compensate for violations of the constant image brightness assumption. According to this assumption, intensities of corresponding points in two or more images of the same scene should be equal. The assumption relates to works in optical flow estimation (e.g., Negahdaripour, 1998; Negahdaripour and Yu, 1993). HSWP supposes that errors in the constant image brightness assumption can be described by a nonlinear monotonically increasing function that uniquely maps intensity values in the first image to intensity values in the second image. HSWP is based on matching one histogram onto another and supposes matching intensities one-to-one (identity), one-to-many (expansion), many-to-one (contraction), or many-to-many (expansion or contraction) (see Figure 7).

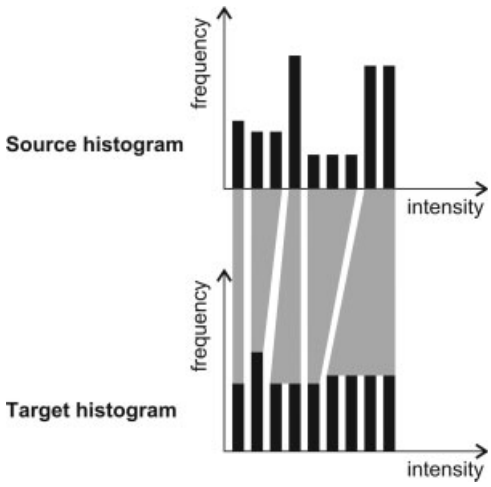

Fig. 7. Examples of matching intensities of two histograms; from left to right: 1-1 (identity), 2-1 (contraction), 1-2 (expansion), 3-1 (contraction), 2-4 (many-to-many expansion).

HSWP is based on minimization of a cost function. To specify the cost of a matching, let h_m^α and h_n^β represent the frequency of occurrence in the m-th and n-th bin of a histogram of the first and second image, respectively. Then the cost of matching intensity I_m^α of the first image with intensity I_n^β of the second image is defined as

$$C_{1,1}(m,n) = \mid h_m^\alpha - h_n^\beta \mid . \tag{1}$$

This corresponds to one-to-one mapping. Similarly, the cost of a k-to-l mapping is expressed by

$$C_{kj}(m,n) = \left| \sum_{i=0}^{k-1} h_{m-i}^\alpha - \sum_{i=0}^{j-1} h_{n-j}^\beta \right|. \tag{2}$$

The total cost of a matching is defined recursively as

$$\begin{aligned} &C(0,0) = 0 \\ &C(i,j) = \infty,\ (i \le 0, j \le 0, (i,j \ne (0,0))) \\ &C(m,n) = \min \begin{cases} C(m-1,n-1) + c_{1,1}(m,n) \\ C(m-1,n-l) + c_{ij}(m,n),\ (2 \le l \le N) \\ C(m-k,n-1) + c_{kj}(m,n),\ (2 \le k \le M). \end{cases} \end{aligned} \tag{3}$$

where M and N represent the maximum allowed contraction and expansion of the histogram, respectively. The total cost is expressed here for one-to-one, one-to-many, and many-to-one mappings only, but its extension to high order mappings is straightforward. The cost function (3) is efficiently minimized by dynamic programming (Skiena, 1998).

RESULTS

The online method was implemented within Leica Confocal Software (LCS) package using Visual Basic 5.0 based Macro Developer, and the offline method as a

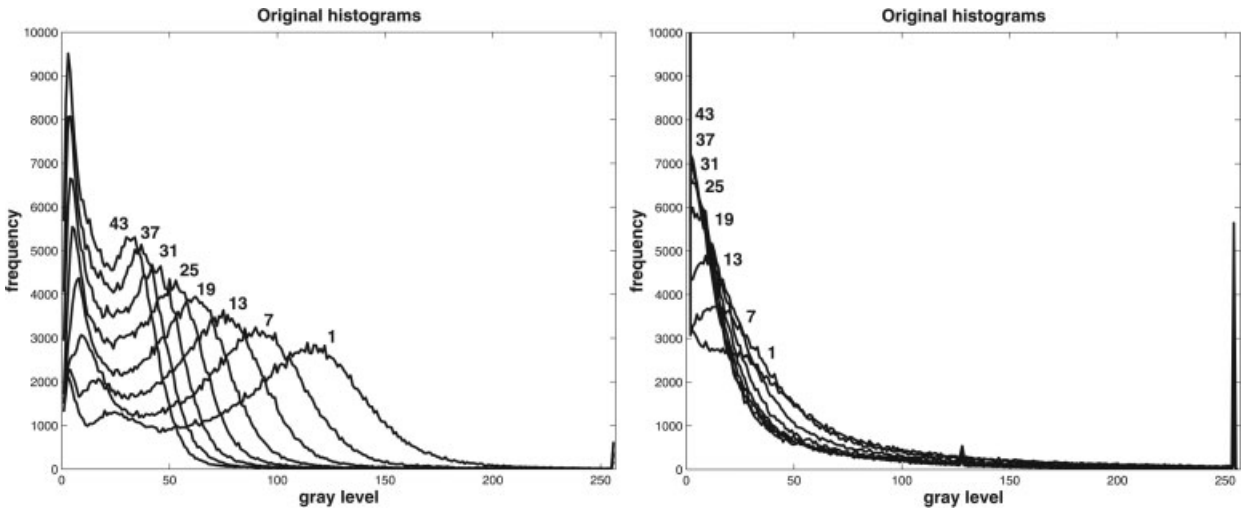

Fig. 8. Original histograms of the subsets of series of optical sections of the human placenta specimen (left) and the rat muscle specimen (right); the right histograms clipped with respect to the maximum frequency at zero gray level. The numbers in the graphs depict numerical order of optical sections in the full series.

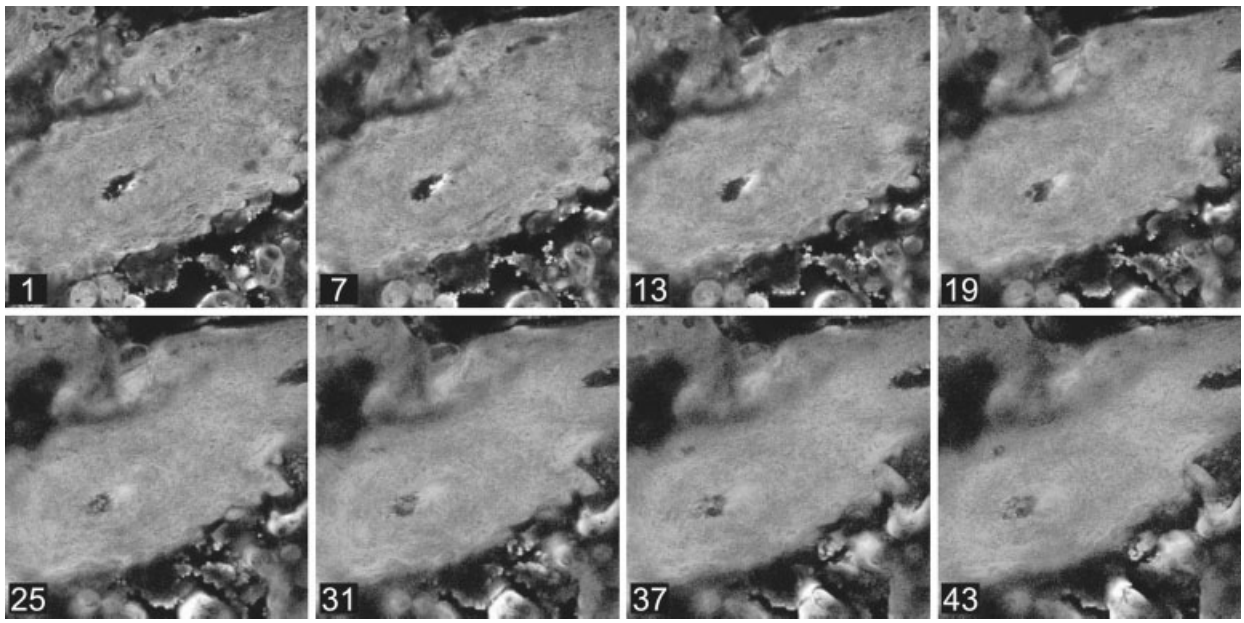

Fig. 9. Subset of a series of confocal optical sections of a human placenta corrected by the offline method after image acquisition.

specialized plug-in of the modular software package Ellipse (ViDiTo, Slovakia, www.vidito.com) in the C++ language. This package is intended for the processing of biological 2D and 3D images.

First, the test specimens were captured under standard conditions, i.e., without using the online correction method. Subsets of the series of optical sections obtained are depicted in Figures 1 and 2. Note the intensity attenuation and evolving objects in the optical sections in *z*-direction. Figure 8 shows their corresponding histograms that are, for clarity, depicted in one image. The decreasing of contrast and intensity of both series with depth is evident.

The obtained stacks of optical sections were processed by our offline method. Results are shown in Figures 9 and 10. Standard histograms, constructed according to the above mentioned description, are demonstrated in Figure 11. We can see the standard histograms practically span all peaks from Figure 8; therefore, they enhance contrast of individual optical sections, and move the average brightness towards high intensities. Figure 12 shows warped histograms of the optical sections. Shapes of the warped histograms clearly pursue the shape of the standard histograms leading to similar brightness and contrast of resulting optical sections in Figures 9 and 10.

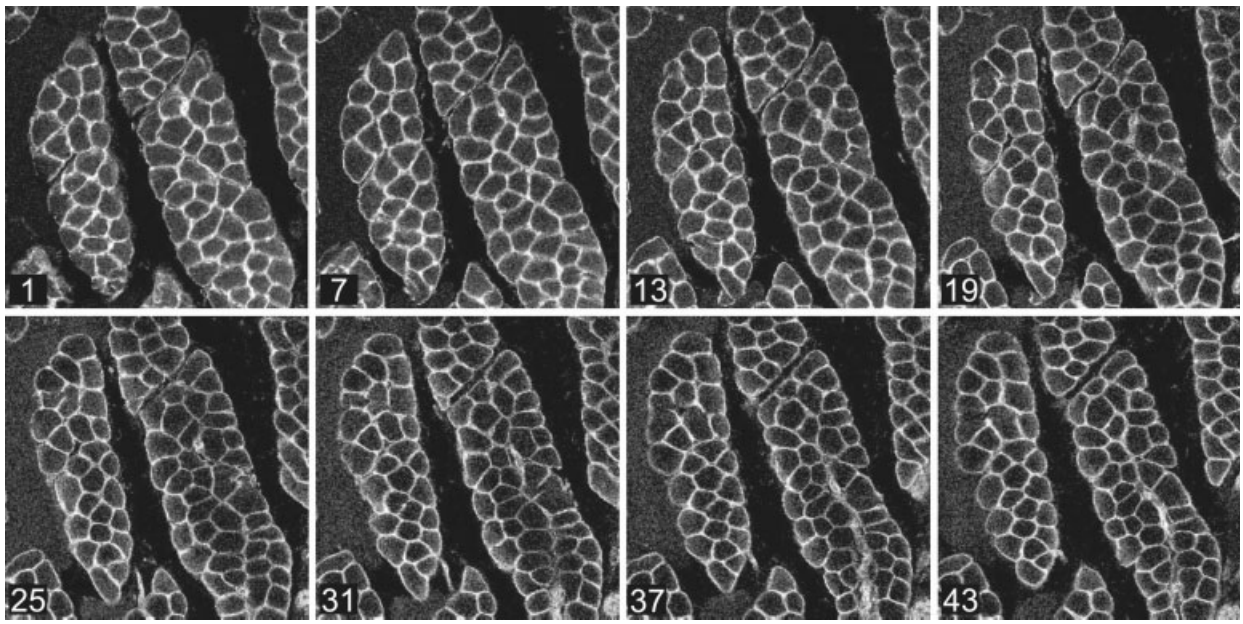

Fig. 10. Subset of a series of confocal optical sections of rat skeletal muscle fibers corrected by the offline method after image acquisition.

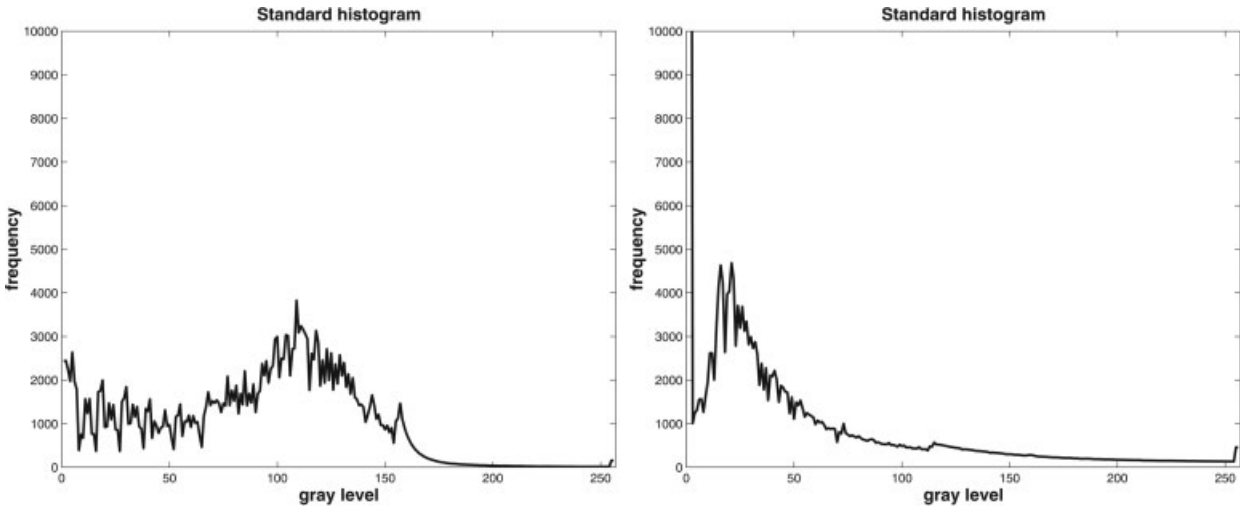

Fig. 11. Standard histograms constructed from the full series of the human placenta specimen (left) and the rat muscle specimen (right); the right histogram clipped with respect to the maximum frequency at zero gray level.

Then, the specimens were captured by using the online method. The first optical section (placenta) and the third optical section (muscle fibers) of the full series, respectively, served as reference images. Results are shown in Figures 13 and 14. Especially in the case of Figure 13, we can see that object details are better expressed by using the online method when compared with Figure 9 obtained by the offline method. This is not surprising, since the online method produces optical sections with broad histograms that cannot be quite compensated by widening narrow histograms of original optical sections using the offline method.

Figure 15 demonstrates an improvement of corrected contrast and brightness of the compensated series over contrast and brightness of the original series. We computed image contrast here (noted C_i for the i-th optical section) as difference between intensity values corresponding to the 90th percentile $p_{90,i}$ and the 10th percentile $p_{10,i}$ of an image histogram:

$$C_i = p_{90,i} - p_{10,i}. \quad (4)$$

The plots of original contrasts (marked 1 in both the graphs) exhibit strong decrease with depth, while the

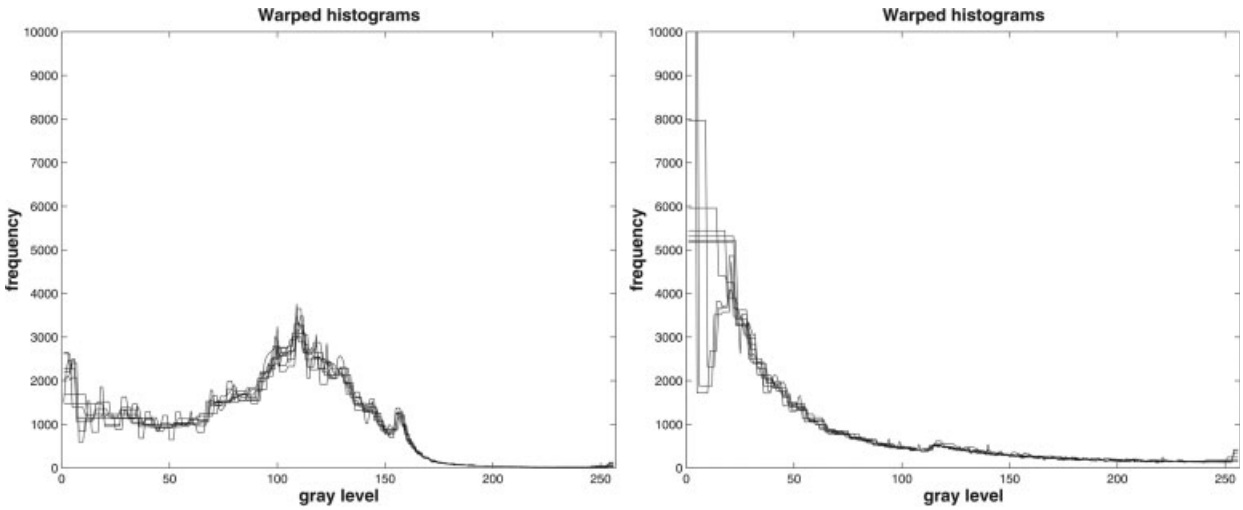

Fig. 12. Warped histograms of the subsets of optical sections of the human placenta specimen (left) and the rat muscle specimen (right); the right histograms clipped with respect to the maximum frequency at zero gray level.

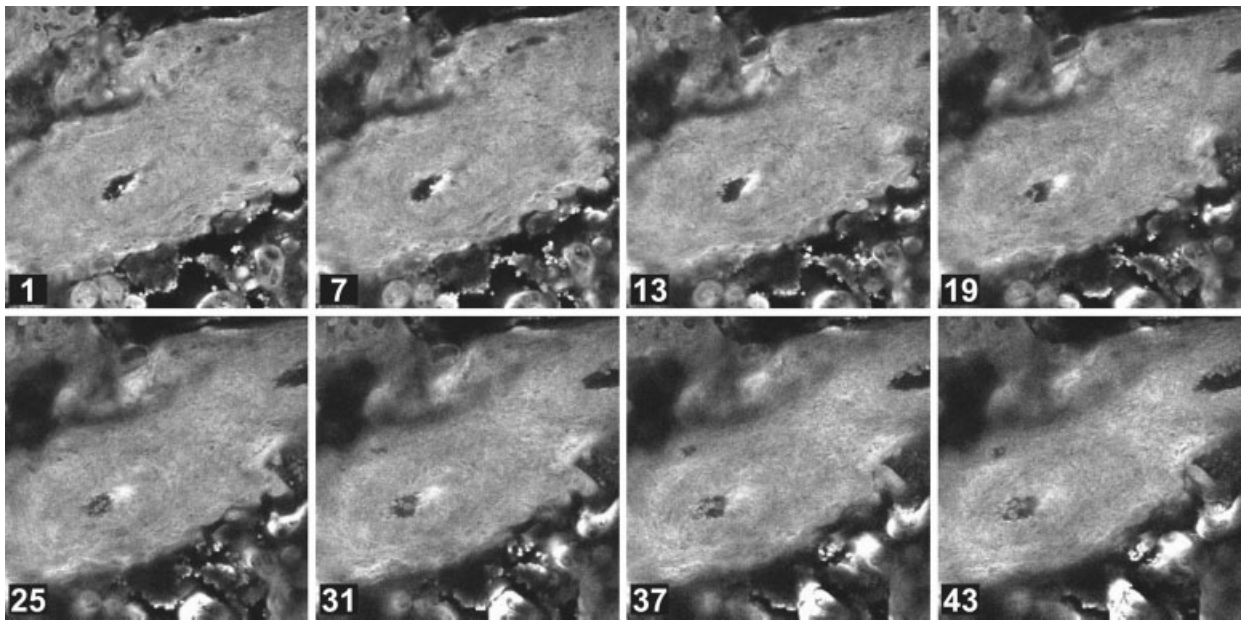

Fig. 13. Subset of a series of confocal optical sections of a human placenta corrected during image acquisition by the online method.

plots of online (2) and offline (3) corrected contrasts are more constant. The image mean intensity curves are also shown. Again, the plots of mean intensities without correction (4) show important brightness decrease, but the plots with online (5) and offline (6) corrections become more constant.

Resulting brightness and contrast of the series of rat skeletal muscle fibers corrected by the offline method (lines 3 and 6 in Figure 15-right) are higher than in the case of the online method. This is caused by the broader standard histogram (Fig. 11-right) and by its mean intensity set around higher intensity when compared with the histogram of the reference optical section used by the online method.

IMPLEMENTATION REMARKS

Remark 1: The optimization strategy applied in the online method is a relatively simple n-step-search. We spent some effort to find out a more efficient strategy, like methods mentioned by Press et al. (1999). However, the used optimized function has many local minima in which the methods get usually trapped. Another fact making the optimization difficult is the slight instability of optical sectioning using a CLSM. When the same confocal plane is scanned repetitively, not

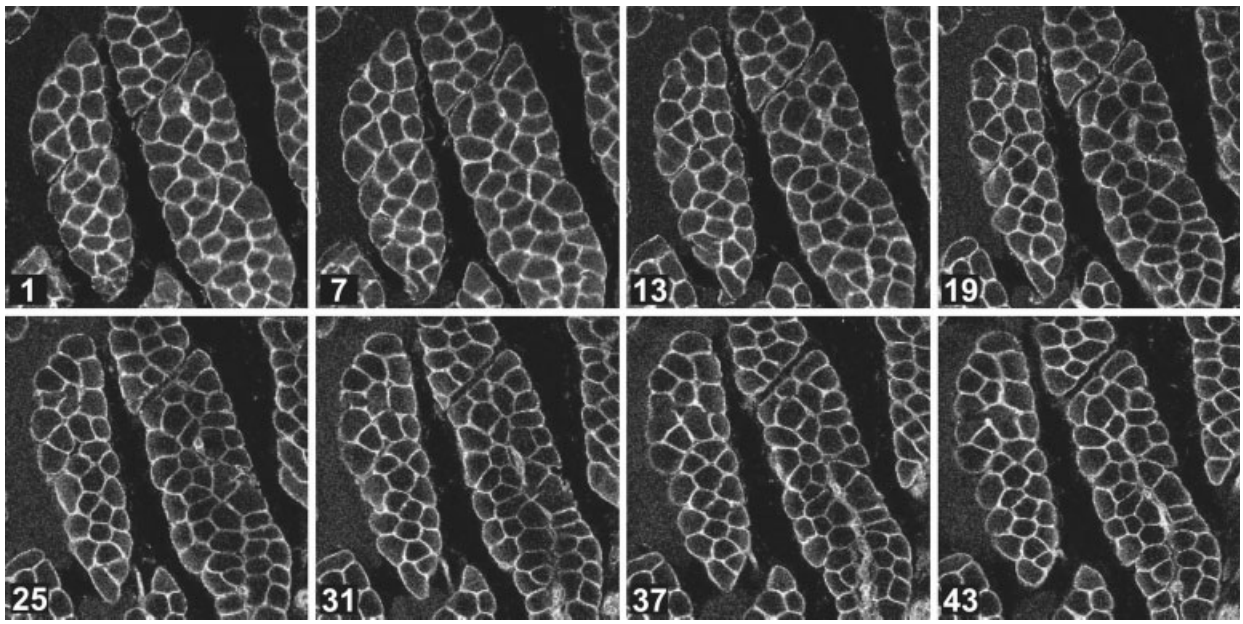

Fig. 14. Subset of a series of confocal optical sections of rat skeletal muscle fibers corrected during image acquisition by the online method.

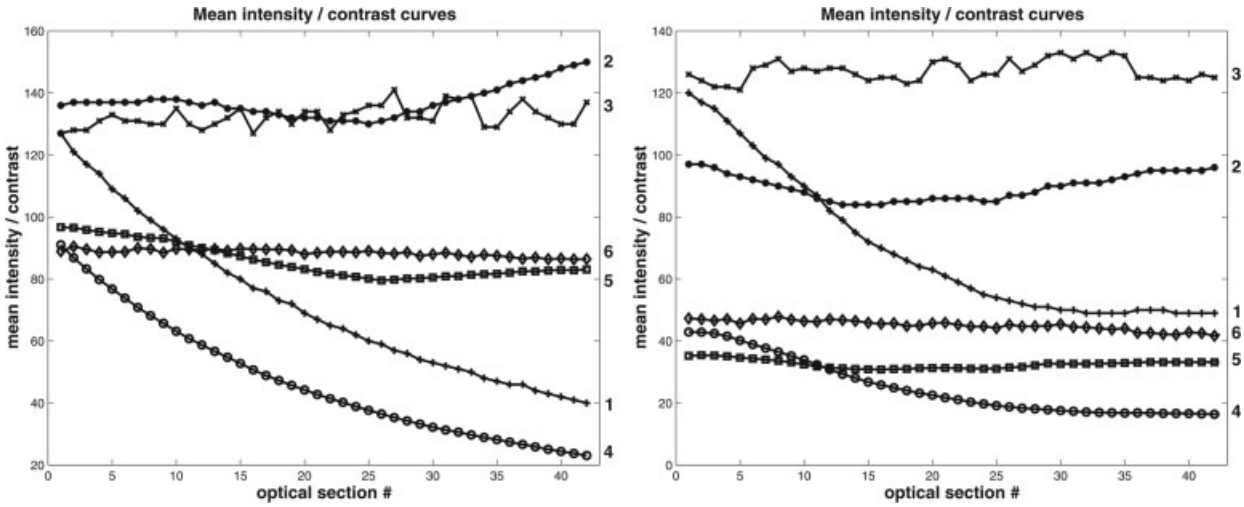

Fig. 15. Original contrast (line 1), contrast corrected by the online method (line 2), contrast corrected by the offline method (line 3), original mean intensity (line 4), mean intensity corrected by the online method (line 5), mean intensity corrected by the offline method (line 6); left: the human placenta series, right: the rat muscle fibers series.

exactly the same value of mean intensity of the captured optical section is usually obtained, because of possible photobleaching and the fact that the focused confocal planes may not be fully identical. Thus, we chose n-step-search as suitable, robust, and fast optimization strategy.

Remark 2: Construction of a standard histogram is designed for increasing overall brightness and contrast of optical sections through a stack while maintaining relative frequencies of gray levels in the stack. However, although the standard histogram improves both the brightness and contrast, it may happen the corrected images are still darker than we would expect. This occurs especially if images containing otherwise dark objects include small bright areas. In real practice, this scenario is not too frequent, but represents an event that should be considered and solved.

Our experiments showed that the distance $|L_{10} - L_9|$ of the standard scale was the highest in most cases and had the highest influence from all other considered distances on the resulting brightness and contrast of the standard histogram. To have a possibility to control resulting brightness and contrast, we added a parameter that controls the length of $|L_{10} - L_9|$ distance.

We applied this parameter during offline correction of the series of optical sections of a human placenta. By

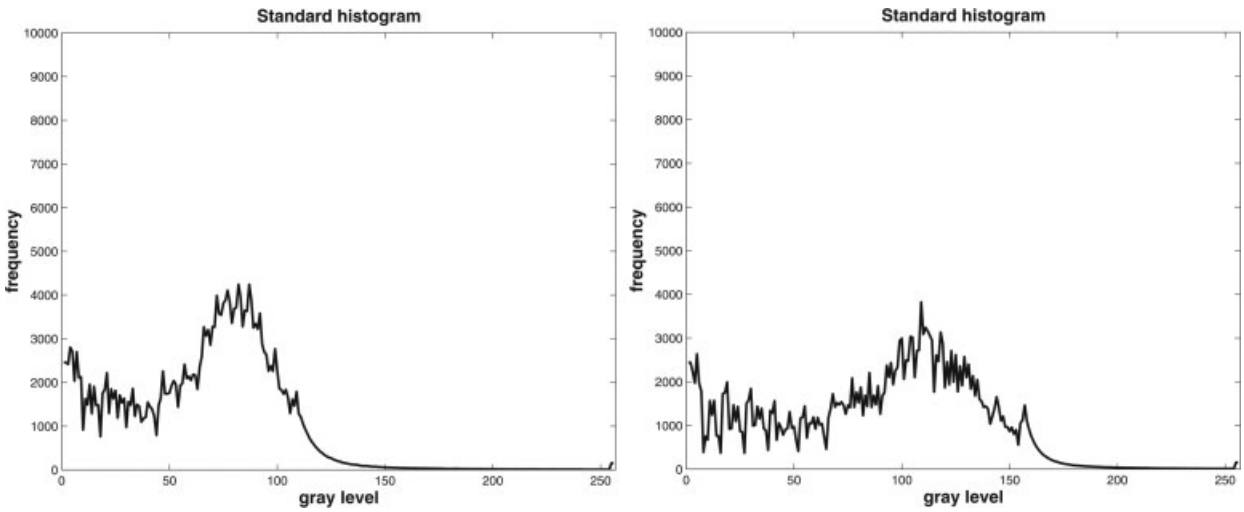

Fig. 16. Standard histograms before and after applying a parameter controlling the distance of $|L_{10} - L_9|$ mentioned in the text.

decreasing the length of $|L_{10} - L_9|$ distance to 50% of the original value, we obtained the standard histogram depicted in Figure 11-left. Figure 16 compares the standard histograms before and after applying the above mentioned parameter. High $|L_{10} - L_9|$ distance was caused in this case by bright saturated objects in the right bottom corner of otherwise dark optical sections captured from deep confocal planes (see Figure 1).

Remark 3 concerns minimization of the cost function (3) by using dynamic programming. This is still a relatively computationally demanding task. Dynamic programming requires filling in a table of 256 × 256 size (256 gray scale levels), using the above described recursive function (Skiena, 1998). HSWP of one slice then requires about 15 s (Pentium 4, 2.8 GHz).

To speed up the computing process, we implemented dynamic programming in a pyramidal set-up, see Figure 17. In the first step, gray levels of an optical section are reduced to 64 levels only, and a 64 × 64 table is filled in by using the cost function (a small square on the left). After finding a path in the table corresponding to optimal HSWP (a black line in the small square on the left), this path is rescaled to a 256 × 256 table, and dynamic programming runs only in the vicinity of the rescaled path (a dark gray area in the big square on the right). Then, the optimal path of HSWP for 256 gray levels, i.e., a transfer function between two histograms, is found (a black line in the big square on the right). This simple approach speeds up the calculations approximately five times.

Remark 4: Values M and N of the cost function (3) represent the maximum allowable contraction and expansion of the histogram, respectively. Commonly, these values are set to maximum, i.e., 256 gray levels. However, especially high value of N, i.e., expansion of one or more gray levels of an original histogram to many gray levels of a resulting histogram, can cause a "thresholding" effect in images. This means that objects in images do not have smooth borders, but there is a sudden jump in intensities between the objects and the background. By manipulating with the parameter

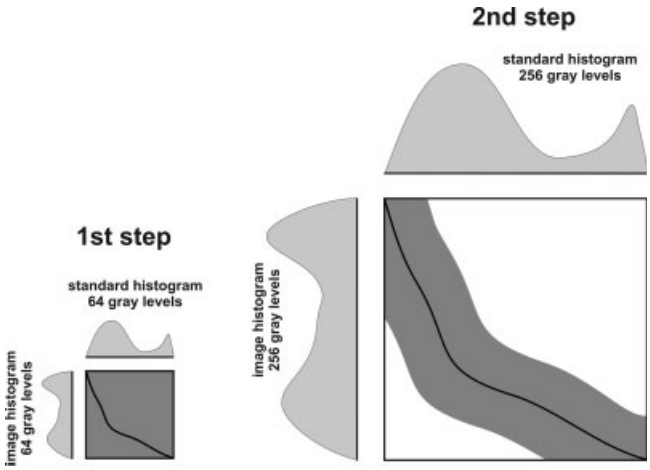

Fig. 17. Pyramidal set-up of dynamic programming computation.

N, we are able to control how much a resulting histogram can be warped and, thus, to eliminate the "thresholding" effect.

Remark 5 deals with regularization, i.e., stabilization, of warped histograms of optical slices in z-direction. In the original article (Cox et al., 1995), authors permitted matching intensities up to one-to-many and many-to-one only. Many-to-many matchings were not allowed (see also Figure 7). According to our experiments, this set-up causes discrepancies among warped histograms of optical sections from different optical planes within the same specimen. The rule was too strict. Therefore, we allowed in our algorithm matching intensities up to three-to-many and many-to-three (high order mappings), which stabilized the warped histograms of optical section in z-direction and improved the visual results, see comparison of contrast and mean intensity curves before and after applying high order mappings in Figure 18.

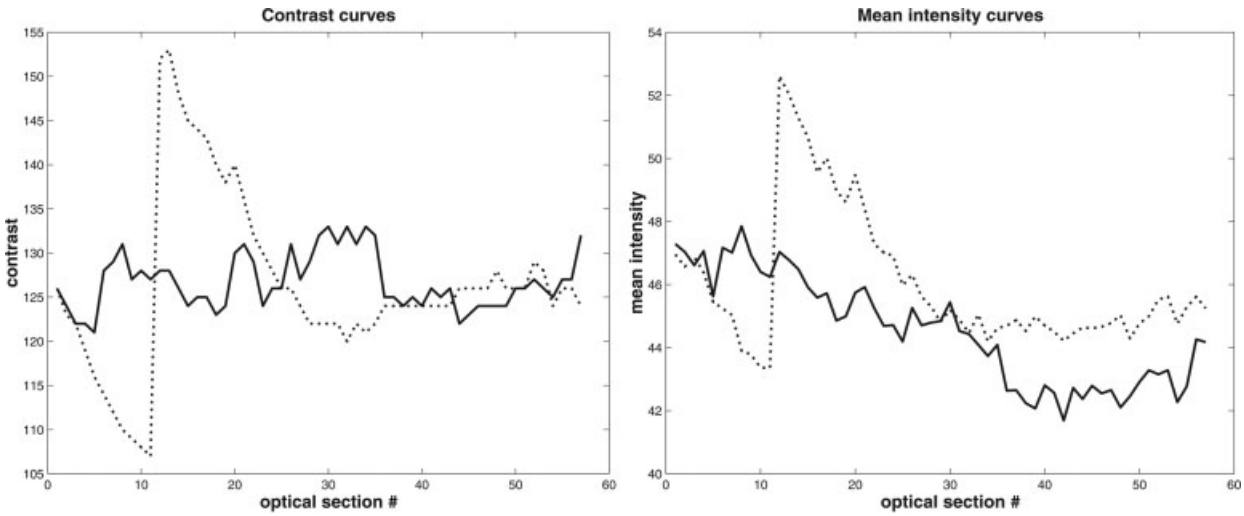

Fig. 18. Comparison of contrast and mean intensity curves of the offline corrected series of the rat muscle fibers specimen using one-to-one, one-to-many, and many-to-one mappings (dotted lines) versus using mappings up to three-to-many and many-to-three (full lines). Note more stable lines in the case of the high order mappings.

DISCUSSION

The goal of this work was to compensate for the intensity and contrast loss with depth inside a specimen in confocal microscopy. For this purpose, we developed and implemented both an online method and offline method. It was shown that the methods yield satisfactory results for real confocal data.

In the proposed methods, we used other approach than modeling the light attenuation by the exponential decay law, applied most often in the literature. Instead, we considered that individual light loss components—namely inadequate specimen staining, light aberration, and photobleaching—contribute to overall light attenuation with depth. Each of our methods uses one single parameter that comprises all light loss components and carries information about the light attenuation. The parameter used in the online method is the image mean intensity value whereas in the offline method it is the image histogram. By this concept, the methods become robust, general, and in the case of the offline method its using is not restricted to confocal microscopy only, but it can be used in any area where offline adjustment of image light conditions is required.

Using the online method is especially highly recommendable, since the improvement of optical sections, particularly restoration of details in images, is generally better when compared with the offline method. However, from practical reasons, using the online method might not be always possible; it increases time spent by acquisition of optical sections from a specimen, because the selected subset of confocal planes tested during optimization ("testing shots") must be scanned repetitively. This effect can be partially eliminated by using low resolution optical sections during optimization and choosing high resolution of optical sections for obtaining the resulting series. Another negative effect of the repetitive scanning can be the faster bleaching of used fluorochromes.

The online method is directly applicable on Leica confocal microscopes using Leica Confocal Software (LCS) package. It requires having the LCS package installed together with Macro Developer option. Source codes are available on demand from the corresponding author.

The offline method has to be used if only acquired data and not the specimen is available. The method is computationally fast ($\sim$2 s per one optical section using Pentium 4, 2.8 GHz) and works best if objects in all optical sections of a series cover approximately the same area. In the opposite case noise hidden in the background might be highlighted.

In the case of images captured in more channels, prior to applying the offline method, individual channels must be separated. After the intensity correction, the channels are again merged. These operations are performed automatically by our program. Optical sections captured by a CLSM are also more or less degraded by noise that can be eliminated, for example, by median filtering. When the online method is used, noise filtering by averaging rows of optical sections during scanning is possible in our macro using features of the LCS package.

Our experimental results show the demonstrated series of sections restored by either method are characterized by more constant curves of image contrast and mean intensity when compared with the original series. Especially, the series of human placenta represented a difficult example exhibiting very strong light attenuation of the main object with depth while small areas of images became bright in deep layers.

According to our trials, both presented algorithms are able to work on various kinds of data sets including sparse stained specimens, specimens with strong contrast and brightness attenuation, or specimens showing tiny objects or sparse structures of objects. We tested both the online and offline method successfully on more than 30 series of optical sections captured from various types of specimens. The results confirmed the stability and applicability of the algorithms in practice.

ACKNOWLEDGMENTS

We thank Dr. Marie Jirkovská (Institute of Histology and Embryology, 1st Faculty of Medicine, Charles University, Prague, Czech Republic) for providing us the human placenta specimen and Prof. Ida Eržen and Dr. Vita Čebašek (Institute of Anatomy, Medical Faculty, University of Ljubljana, Slovenia) for preparing the rat muscle specimen.

REFERENCES

Čebašek V, Kubínová L, Ribarič S, Eržen I. 2004. A novel staining method for quantification and 3D visualisation of capillaries and muscle fibres. Eur J Histochem 48:151–158.

Cox IJ, Roy S, Hingorani SL. 1995. Dynamic histogram warping of image pairs for constant image brightness. Proc IEEE Image Processing 2:366–369.

de Monvel JB, Le Calvez S, Ulfendahl M. 2001. Image restoration for confocal microscopy: Improving the limits of deconvolution, with application to the visualization of the mammalian hearing organ. Biophys J 80:2455–2470.

Diaspro A, editor. 2002. Confocal and two-photon microscopy: Foundation, applications, and advances. New York: Wiley-Liss.

Difato F, Mazzone F, Scaglione S, Fato M, Beltrame F, Kubínová L, Janáček J, Ramoino P, Vicidomini G, Diaspro A. 2004. Improvement in volume estimation from confocal sections after image deconvolution. Microsc Res Tech 64:151–155.

Ghauharali RI, Brakenhoff GJ. 1998. Fluorescence photobleaching-based shading correction for fluorescence microscopy. J Microsc 192:99–113.

Ghauharali RI, Brakenhoff GJ. 2000. Fluorescence photobleaching-based image standardization for fluorescence microscopy. J Microsc 198:88–100.

Gonzales RC, Woods RE. 1993. Digital image processing. New York: Addison-Wesley.

Jirkovská M, Kubínová L, Janáček J, Moravcová M, Krejčí V, Karen P. 2002. Topological properties and spatial organization of villous capillaries in normal and diabetic placentas. J Vasc Res 39:268–278.

Kervrann C, Legland D, Pardini L. 2004. Robust incremental compensation of the light attenuation with depth in 3D fluorescence microscopy. J Microsc 215:297–314.

Liljeborg A, Czader M, Porwit A. 1995. A method to compensate for light attenuation with depth in three-dimensional DNA image cytometry using a confocal scanning laser microscope. J Microsc 177:108–114.

Margadant F, Leemann T, Niederer P. 1996. A precise light attenuation correction for confocal scanning microscopy with O(n4/3) computing time and O(n) memory requirements for n voxels. J Microsc 182:121–132.

Markham J, Conchello JA. 2001. Artefacts in restored images due to intensity loss in three-dimensional fluorescence microscopy. J Microsc 204:93–98.

Negahdaripour S. 1998. Revised definition of optical flow: Integration of radiometric and geometric clues for dynamic scene analysis. IEEE Trans Pattern Anal Mach Intell 20:961–979.

Negahdaripour S, Yu C-H. 1993. A generalized brightness change model for computing optical flow. In: Proceedings of the 4th International Conference on computer vision. May 1993, Berlin, Germany. pp. 2–11.

Nyúl LG, Udupa JK. 1998. On standardizing the MR image intensity scale. Radiology 209P:581–582.

Nyúl LG, Udupa JK, Zhang X. 2000. New variants of a method of MRI scale standardization. IEEE Trans Med Imaging 19:143–150.

Pawley J. 1995. Handbook of biological confocal microscopy. New York: Plenum.

Periaswamy S, Farid H. 2003. Elastic registration in the presence of intensity variations. IEEE Trans Med Imaging 22:865–874.

Press WH, Teukolski SA, Vetterling WT, Flannery BP. 1999. Numerical recipes in C: The art of scientific computing, 2nd ed. Cambridge, UK: Cambridge University Press.

Rodenacker K, Hausner M, Kühn M, Wuertz S, Purkayastha S. 2001. Depth intensity correction of biofilm volume data from confocal laser scanning microscopes. Image Anal Stereol 20 (Suppl 1):556–560.

Skiena SS. 1998. The algorithm design manual. New York: Springer-Verlag.

Sun Y, Bartek R, Robinson JP. 2004. Adaptive image-processing technique and effective visualization of confocal microscopy images. Microsc Res Tech 64:156–163.

Verveer PJ, Gemkow MJ, Jovin TM. 1999. A comparison of image restoration approaches applied to three-dimensional confocal and wide-field fluorescence microscopy. J Microsc 193:50–61.

Wahlby C, Sintorn IM, Erlandson F, Borgefors G, Bengtsson E. 2004. Combining intensity, edge and shape information for 2D and 3D segmentation of cell nuclei in tissue section. J Microsc 215:67–76.

Zhang YJ. 1992. Improving the accuracy of direct histogram specification. Electron Lett 28:213–214.